Characterization of Al/B4C composite materials fabricated by powder metallurgy process technique for nuclear applications

Alexandre Brillon, Justo Garcia, Fanny Riallant, Christian Garnier, Anne Joulain, Yongfeng Lu, Jean-François Silvain

Characterization of Al/B_4C composite materials fabricated by powder metallurgy process technique for nuclear applications

Alexandre BRILLON[a], Justo GARCIA[b], Fanny RIALLANT[b], Christian GARNIER[c], Anne JOULAIN[d], Yongfeng LU[e] and Jean-François SILVAIN[a,e]

[a] *CNRS, Université de Bordeaux, Bordeaux INP, ICMCB, UMR 5026, 87 Avenue du Docteur Schweitzer 33600 Pessac, France,*
[b] *Orano, 125 Av. de Paris, 92320 Châtillon, France*
[c] *Laboratoire Génie de Production, ENIT, 47 avenue d'Azereix - BP 1629 - 65016 Tarbes, France*
[d] *Institut Pprime, UPR 3346, CNRS-Université de Poitiers-ENSMA, 11 Boulevard Marie et Pierre Curie, TSA 41123, Poitiers, F86073, France*
[e] *Department of Electrical and Computer Engineering, University of Nebraska-Lincoln, Lincoln, NE 68588-0511, USA*

Email : alexandre.brillon@icmcb.cnrs.fr ; justo.garcia@orano.group ; fanny.riallant@orano.group ; christian.garnier@enit.fr ; anne.joulain@univ-poitiers.fr ; yflu.email@gmail.com ; Jean-francois.Silvain@icmcb.cnrs.fr

Abstract

Aluminum (Al) matrix composites with boron carbide (B_4C) reinforcements were fabricated by solid state powder metallurgy using the hot-pressing process. Composite materials were fabricated at different volume fractions of B_4C particles, ranging from 2% to 12%, to evaluate the impact of B_4C reinforcements on the thermal and mechanical properties of the composite materials. Thermal properties, such as thermal conductivity (TC) and the coefficient of thermal expansion (CTE), were measured and modeled. The mechanical properties were evaluated by Vickers macro-hardness (HV) and tensile tests to obtain the strain hardening threshold (σ_y), ultimate tensile stress (UTS), and elongation (A) of the developed composites. Microstructures were observed by scanning electronic microscopy (SEM) and transmission electron microscopy (TEM) to show the homogeneity of composites materials with different B_4C contents and to characterize the Al/B_4C interface. This article shows that incorporating B_4C particles until 12% in the Al matrix increased the hardness (+85%) and strain hardening threshold (+55%) of the composite material and decreased the ductility. An increase, up to 8 vol.% B_4C, of mechanical properties which a decrease of the

elongation at rupture is measured. The strain hardening threshold and the UTS strength increased up to 37% and 13%, respectively. For higher B_4C volume fraction, Al/B_4C become more brittle leading to very limited plastic phases. Moreover, both the TC and the CTE decreased as a function of the increase of the B_4C volume fraction; 20% decrease of TC was measured for an Al/B_4C (12 vol.%). The thermal and mechanical properties were correlated with the microstructure of the Al matrix and of the Al-B_4C interfacial zone.

Keywords： aluminum matrix composite**,** boron carbide, thermal properties, mechanical properties, powder metallurgy

Highlights

1. Homogeneous Al/B_4C composite materials were fabricated through solid state powder metallurgy by the hot-pressing sintering process. The Al/B_4C interface was observed by TEM.
2. Experimental values were modeled for thermal conductivity and the coefficient of thermal expansion with the volume fraction of B_4C.
3. Al/B_4C tensile test characterization with different contents of B_4C and mechanical behavior were discussed.

1. Introduction

Nuclear energy has been in continuous progress for years and is a current application for composite materials [1-4]. The transport and storage of spent nuclear fuel requires protective structures to prevent polluting the external environment. Spent nuclear fuel is highly radioactive and generates neutron radiation from nuclear decay [4-5]. To avoid critical accidents and resist extreme conditions, protective materials must be neutron-absorbing and possess adapted mechanical and thermal properties, such as thermal conductivity (TC), to dissipate the heat generated by nuclear materials. The coefficient of thermal expansion (CTE) of materials and, for our example, metal matrix composites has been recognized as one of the most important thermomechanical properties because thermal stability over time is regarded as a critical issue [6-7].

Aluminum (Al) matrix composites (AMCs) reinforced with ceramic particles (Al_2O_3 [8], SiC [9], TiB_2, B_4C) have shown high mechanical performance (e.g., strength [1] and hardness [3]), low CTE, and good wear resistance properties, including low density and relatively low cost [4, 10-11]. Among these ceramic reinforcements, boron carbide (B_4C) is an ideal candidate due to its neutron absorption ability, high strength and stiffness [2] (Table I), good wear [3], high thermal stability (melting point 2450 °C), good TC, chemical resistance, and low density (2.51 g/cm^3) [12-13]. The thermal neutron absorption of B_4C is linked with the thermal neutron absorbing cross section (3837 barn, barn = 10^{-24} cm^2 [5]) of ^{10}B isotope. B_4C reinforced Al composites have been adopted in the nuclear industry. Al has been chosen due to its high TC, good mechanical properties, low density (2.71 g/cm^3), and simple machinability, which allows a combination of properties not found in conventional materials [14]. Moreover, the presence of Cu, Mg, or Si in Al alloys improve the mechanical properties of Al but lower its ability to conduct heat [15-16]. Therefore, unalloyed Al is preferred to fulfil the specifications of the nuclear industry and, specifically, to achieve a thermal conductivity as high as possible.

Al matrix composite materials are fabricated by either the liquid-state process (e.g., stir welding [2], stir casting [4], squeeze casting [11], infiltration) [17]) or the solid-state process (e.g., powder metallurgy) [4, 6, 18]. The final macroscopic properties of metal matrix composites are linked with the intrinsic properties of the matrix (M), reinforcement (R), M-R interfacial zones, porosity level, and homogeneity of the distribution of the R inside the M. Thus, a strong chemical interface between the M and R should lead to optimal property transfer and physical and mechanical stability during the material's lifetime, where low porosity and homogeneous R distribution lead to optimal physical and mechanical properties. Therefore, each of these points has to be carefully challenged and are mainly linked with the fabrication process.

Homogeneity is often a challenge in the liquid sintering processes due to the density difference between the M and R and the complexity of mixing in the liquid sintering process. Whereas composite materials fabricated by powder metallurgy show a good dispersion of reinforcement particles in the Al matrix. On the other hand, the weak chemical affinity, in solid state, between Al and B_4C particles limits the elemental diffusion and

interphase formation even if Al_3BC and AlB_2 are thermodynamically stable in solid state range [3, 19-20]. In fact, the Al_3BC phase can form above 550 °C at the Al-B_4C interface in solid state, improving final mechanical properties [3, 21].

Microstructure of Al/B_4C materials and of Al-B_4C interfacial zones are important issue for mechanical properties and so commonly characterized in literature [21-22]. For example, the fabrication of such composite materials, using liquid route process, leads to interfacial reaction between Al and B_4C [23]. Oppositely, in the solid route process, chemical interfacial reaction is low leading to poor interfacial property transfer [1, 23-24]. Several studies show that the incorporation of carbide forming element such as Cr [20] or Ti [22], either in solid and liquid state, improve interfacial adhesion due to the formation of interfacial carbide species. Moreover, the addition of B_4C particles, in an Al matrix, leads to an increase of mechanical properties with a strengthening of the material. The rupture mechanisms have been studied by Soliman *and al* [25], where the initiation of fractures is mainly carried out at the Al-B_4C interface.

Neutron absorption is the main property desired for this nuclear material even if other mechanical and physical properties are also important. Obviously, the volume fraction of B_4C materials is the major parameter to adapt all of these properties. Due to the intrinsic properties of B_4C, increasing the B_4C content will increase the mechanical and neutron absorption [1] of the composite material but decrease its thermal properties.

Table I: Mechanical characteristics of ceramic reinforcement

	Vickers Hardness (GPa)	Young's modulus E (MPa)	Ultimate Tensile Strength UTS (MPa)	Elongation A (%)
B_4C	37-47 [26]	445 [26]	260 - 560 [13]	< 0.1 [13]
Al_2O_3	18-21 [26]	400 [26]	267 [27]	0.1-0.2 [27]
SiC	20-35 [26]	480 [26]	250-500 [28], [29]	~ 0.1 [28]
TiB_2	25-35 [26]	560 [26]	-	-

In the present work, Al/B_4C composite materials with different contents of B_4C (2 - 12 vol.%) were successfully fabricated by solid state powder metallurgy via conventional hot-pressing to fulfill the requirements of the nuclear industry. To improve interfacial reaction zone between Al and B_4C, Al/B_4C composite materials were densification in solid state at 620 °C, near to the melting temperature of Al, using small particles of B_4C. TC and CTE of Al/B_4C composite materials, with different B_4C content, are measured. The mechanical and thermal properties were investigated and correlated with the composite microstructure. The theoretical thermal conductivity was estimated using the Hasselman-Johnson equation, slightly modified to account for the change in the TC of Al due to Boron (B) diffusion.

2. Experimental

2.1. Materials and methods

Gas-atomized 1080 Al spherical powder (ULTD0065, Hermillon powders, FRANCE, Fig. 1-a) with an average diameter of 7 µm was used as the matrix powder. Polygonal B_4C powder (Hot-pressed Grade, Panadyne, USA, Fig. 1-b) with a bimodal population (30 vol.% of an average of 500 nm and 70 vol.% of an average of 5 µm) was used as the reinforcement.

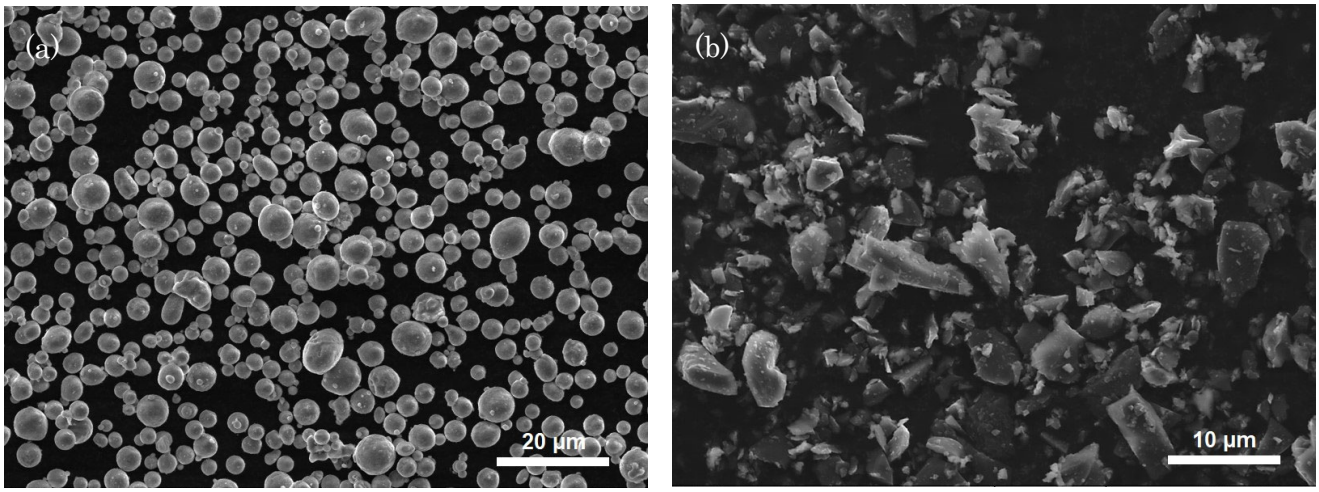

Figure 1. SEM micrographs of starting materials; **(a)** Al powder, **(b)** B_4C powder.

Table II: Material chemistry of Al and B_4C powders

Material	**Al**	**O**	**Fe**	**Si**		
Al powder	Balance	0.3	0.1	0.1		
	B_4C	**B_2O_3**	**Free B**	**Free C**	**Al**	**Fe**
B_4C powder	Balance	0.22	0.24	1.27	0.05	0.20 max

The powders were sieved to 50 µm to remove agglomerations and then mixed at selected proportions by an acoustic mixer (LabRAM II, Resodyn) for 2 min at 80 g. The powder mixture was placed in a steel mold. Composite materials were fabricated in solid state sintering by hot-pressing for 30 min at 620 °C (below the melting point of Al (660 °C)), using induction heating and under a uniaxial compressive stress of 60 MPa. The chamber was put in a primary vacuum (~0.1-1 Pa) to prevent oxidation. The volume fraction of B_4C was controlled between 2 and 12 vol.% by steps of 2 vol.%. Temperature was monitored by a K-type thermocouple located 2 mm from the sample in the steel mold (Fig. 2-a).

Composite materials were fabricated in cylinder form (Ø 10×5 mm^3) for thermal conductivity measurements and CTE investigations and in ingots of size 100×60×4 mm^3 for mechanical properties. Tensile test specimens were machined by a high-pressure water jet, allowing clean and precise cuts while minimizing the thermal stresses induced by the machining step, in a geometry according to ISO 527-2 (5A) standard (Fig. 2-b).

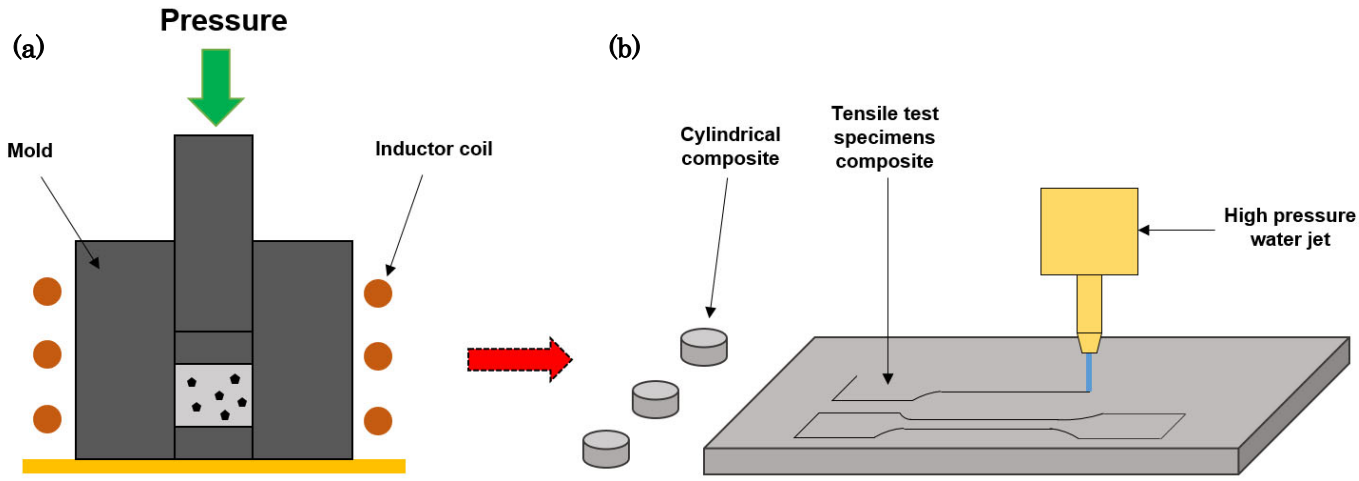

Figure 2. **(a)** Schematic hot-pressing method by induction heating and uniaxial compressive stress of solid-state sintered Al/B_4C composites, **(b)** Two geometry of samples have been fabricated: cylindrical form for thermal characterization and ingot were machined by a high-pressure water jet for tensile test specimens.

2.2. Characterization

Microstructural characterization of Al/B_4C composites was carried out by scanning electron microscopy (SEM, Tescan, VEGA © II SBH) and transmission electron microscopy (TEM, TALOS F200S G2 FEI Inc.) for interface Al-B_4C analysis. A Transmission Electron Microscope (TEM) thin foil was extracted and then thinned by focused ion beam (FIB) with a Helios Nanolab G3 CX, FEI Inc.

The CTE of Al/B_4C composite materials was measured with a dilatometer (NETZSCH DIL 402, PC ®) in two cycles from 50 °C to 300 °C with heating/cooling rates of 2 °C/min under argon gas flow. The average CTE values ranged between 50 °C and 250 °C and were recorded during the cooling step of the second cycle to avoid thermomechanical relaxation of the material.

The thermal conductivity of the Al/B_4C composites materials (k_c) was determined indirectly by measuring the thermal diffusivity (λ), heat capacity (C_p) and density (ρ) of the Al/B_4C composites materials. The thermal conductivity was estimated using the following equation:

$$k_c = \lambda(T) \times \rho \times C_p(T) \quad (1)$$

The thermal diffusivity of Al/B_4C composite materials was measured by the laser flash method (NETZSCH LFA 459, MicroFlash) at 30 °C, 150 °C, and 300 °C under air. The measured standard deviation was close to 5 %. The heat capacity was measured by Differential Scanning Calorimetry (DSC 8000 Pyris Diamond PERKIN ELMER) at 30 °C, 150 °C, and 300 °C for Al powder and B_4C powder. The heat capacity of Al/B_4C composite materials was determined by simple mixture law:

$$C_p(T) = V_{Al} \times C_pAl(T) + V_{B4C} \times C_pB_4C(T) \quad (2)$$

where V_i is the weight fraction of the powder i and C_p i (T) is the heat capacity at temperature T of powder i.

The theoretical density of the composites was calculated using the mixture rule. The experimental density of

the Al/B_4C composites was estimated using the Archimedes principle, which only considers composites with closed porosity.

Hardness values are averages of 10 measurements determined by indenting a pyramidal diamond piece with force of 5 kgf (49 N) during 15 s, on polished surface (WILSON Hardness, Vickers 452 SVD). The dimension (D) of the imprint on the surface allow to determine the hardness of the composite material, using the following formula:

$$HV = 0{,}1891\frac{F}{D^2} \quad (3)$$

where HV is the hardness Vickers, F the force applied and D, the average dimensions of diagonals of imprint. Mechanical tensile tests were performed according to the ISO 6892-1 / SPE-20-028210-000-1.0 standard on the specimens at room temperature. Yield tensile strength (σ_y) and ultimate tensile strength (UTS) were determined by stress-strain curves. Each physical measurement of the Al/B_4C composites is an average of 3 samples that were prepared by mechanical polishing with waterproof abrasive silicon carbide papers (#500, #800, #1200).

3. Results and discussion

3.1 Microstructure

Fig. 3 shows the microstructure of Al/B_4C composites analyzed by SEM with different B_4C contents. The grey phase represents the Al matrix, and the black phase represents the B_4C particles. On the micrographs, the quantity of B_4C may seem higher due to the important difference in hardness between Al and B_4C leading to a low surface roughness during polishing resulting from a decohesion of the Al matrix between the B_4C particles. Bimodal population of B_4C reinforcements are observable in the microstructure. The dispersion of the B_4C reinforcement in the matrix is good, and the porosity is not observable at this scale of analysis.

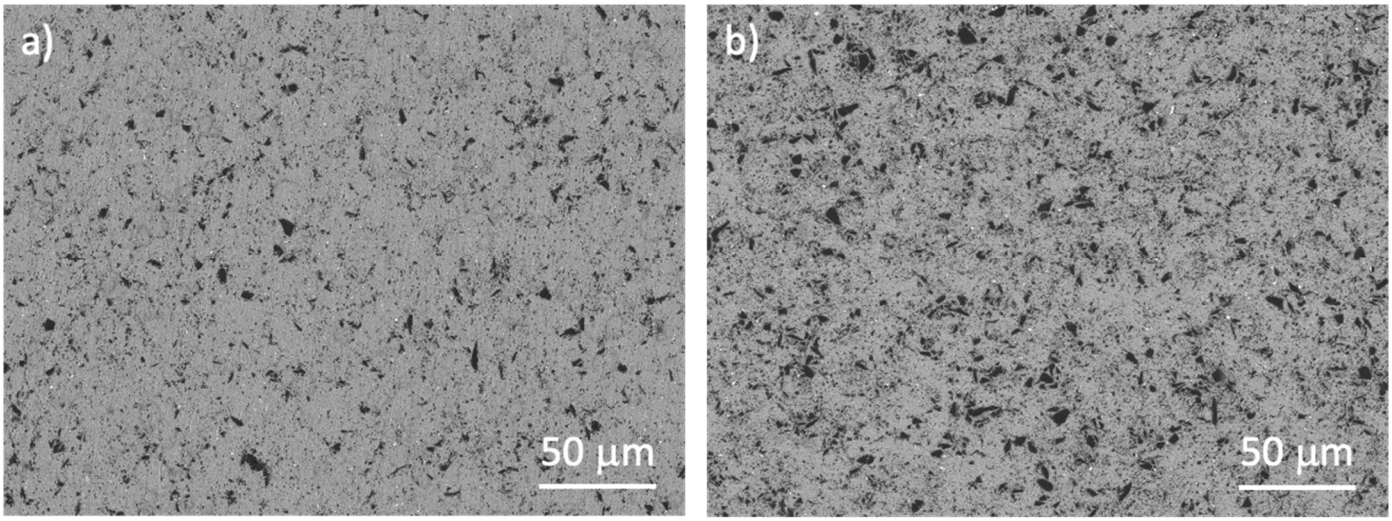

Figure 3. SEM Micrographs of Al/B_4C composites in backscattering electrons for **(a)** 4 vol.% B_4C and **(b)** 10

vol.% B_4C.

TEM analysis was performed on Al/B_4C composite materials with 10 vol.% of B_4C. Fig. 4 shows TEM analysis of the Al/B_4C materials. Fig. 4-a presents a typical micrograph of the Al/B_4C material, using HAADF, acquired from the focused ion beam (FIB) that prepared the sample. Darker contrasts are linked to the B_4C particles and brighter ones represent the Al grains. The white contrast, which can be observed between 2 Al grains, is associated with Al oxide material as it can be seen on Figs. 4-b, and c. At this scale of observation, no porosity can be observed at the interface between the Al grains and the B_4C particles. As it can be seen on the oxygen maps, Al oxide particles, with sizes up to 200 nm, can be randomly observed, mainly at the Al-Al powder boundaries. These Al oxide particles can be attributed to the native Al oxide present on the surface of each Al particle (with thicknesses ranging from 1 to 3 nm) and on possible Al oxide particles present inside the initial Al powders. The Al grains of the composite material reinforced with 10 vol. % of B_4C do not appear deformed after hot-pressing. This behavior may be associated with 1) the possible evolution of the Al matrix's thermal conductivity induced by the formation of Al-B solid solution (i.e., the hardness of Al may also be affected by the diffusion of B inside Al, so the non-deformation of the Al grains will be correlated with the increased hardness of Al (see the thermal properties paragraph)) and 2) the evolution of the mechanical properties of such materials going from ductile for pure Al to fragile for Al/10vol. % B_4C (see the mechanical properties paragraph).

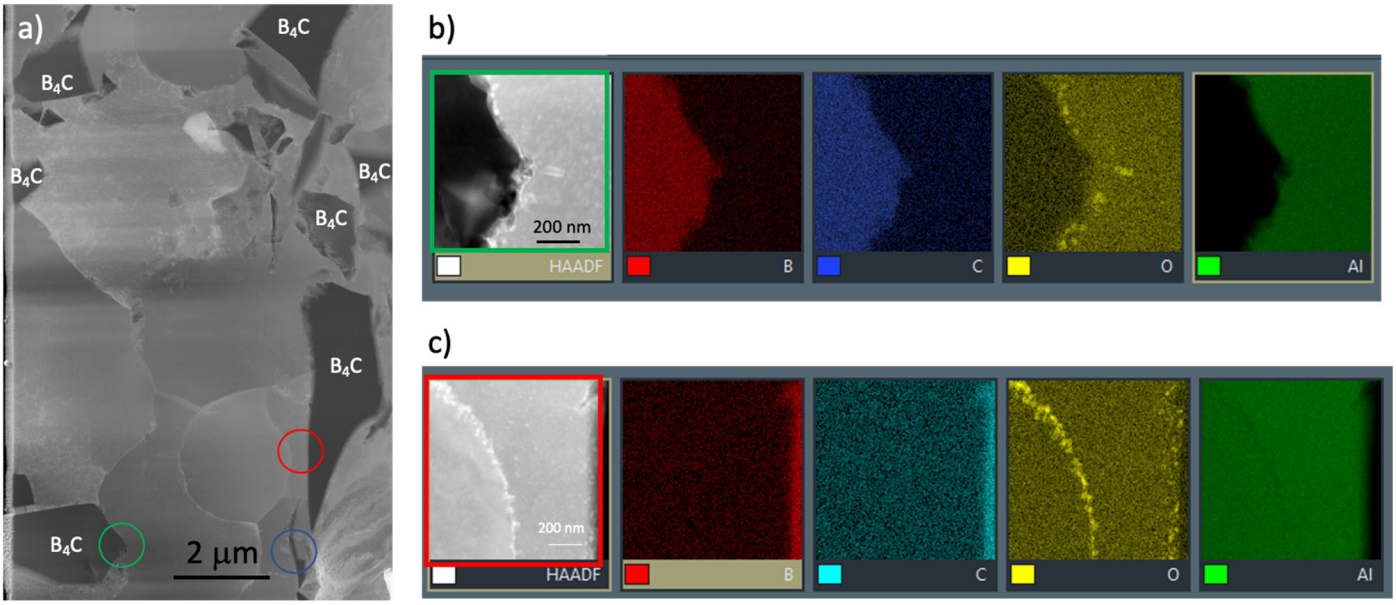

Figure 4. TEM micrographs of Al/B_4C composite material; **(a)** typical imaging of Al/B_4C composite slide **(b)** HAADF imaging and B, C, O, and Al EDX maps at Al-B_4C interface **(c)** HAADF imaging and B, C, O and Al EDX maps at Al-Al grain boundaries.

Figs. 4-b and c show HAADF imaging and corresponding B, C, O, and Al EDX maps (circles with corresponding colors show the localized analysis in Fig. 4-a whereas Fig. 5 shows higher magnification observation at the Al-Al and Al-B_4C interfacial zones. Based on these figures, segregated Al-O particles, with sizes ranging from 10 to 20 nm, can be observed on some Al-Al powder boundaries (see Fig. 5-a (white zone)). The transition between the continuous Al-O film (present on the surface of each Al particles), with a thickness of 1 to 3 nm, to the Al-O particles, after hot densification, is unexplained but the temperature of densification (620 °C) and the pressure (60 MPa) are too low to allow the growth of such particles. Al-O rods (see Fig. 5-b blue arrows) are also visible at the Al-B_4C interface with the presence of some B and C agglomerates (see Fig. 5 (EDX map) white circles). This precipitate is surely related to the Al-O particles also present at the same location. According to the literature, Al_3BC intermetallic can be expected [20-21, 30].

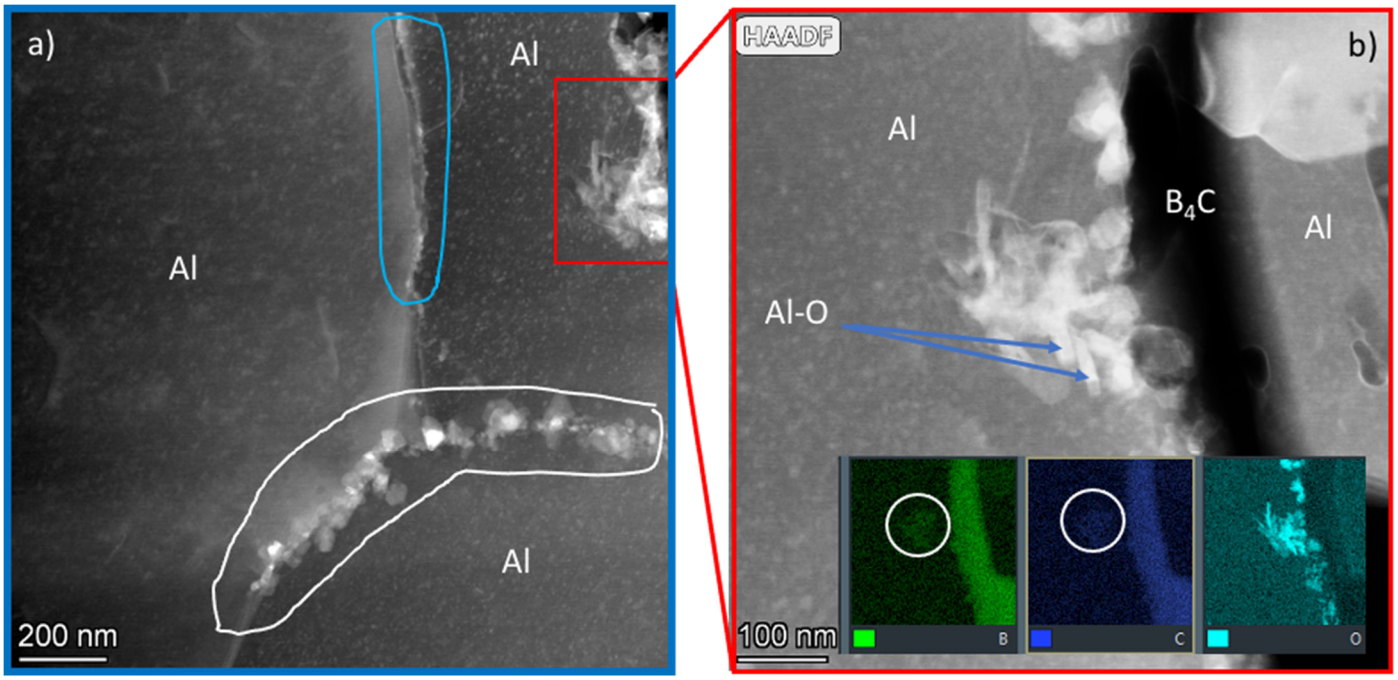

Figure 5. **(a)** Bright field micrograph of the interface between Al grains, and **(b)** HAADF micrograph of Al/B_4C interfacial zone and B, C, and O EDX maps.

3.2 Thermal properties

Pure Al and pure B_4C were fabricated by powder metallurgy and characterized to determine its reference thermal properties. Al materials were prepared by hot-pressing under the same conditions as the composite material. B_4C materials were fabricated by spark plasma sintering [12, 31] at 2000 °C with a heating rate 100 °C/min for 10 min. A pressure of 100 MPa was initially applied and maintained until the end of the temperature stage. Both materials have a relative density greater than 99 %. The physical properties are given in Table III. The TC of the sintered Al powder was lower than the high purity Al reported in the literature (239 W/m.K at room temperature). This is mainly attributed to the amorphous Al_2O_3 and other impurities present on the

surface of the Al powders.

Table III: Physical properties determined for pure Al and pure B_4C

Materials	α (10^{-6} K^{-1})	k (W/m.K)			C_p (J/g.K)		
	T = 50 - 250 °C	T = 30 °C	T = 150°C	T = 300 °C	T = 30 °C	T = 150°C	T = 300 °C
Al	26,2	226	229	228	0,904	0,966	1,030
B_4C	5,5	32	28	24	0,973	1,373	1,682

3.2.1 Thermal conductivity of Al/B_4C composite materials

Fig. 6 shows the thermal diffusivity (TD) of Al/B_4C composites at 30 °C, 150 °C and 300 °C for a B_4C volume fraction ranging between 0 and 12. Whatever the measured temperature, the TD of the Al/B_4C composite material decreases when the B_4C volume fraction increases. Also, for a given B_4C volume fraction, the TD of the composite material decreases when the measured temperature increases. This phenomenon is associated with equation (1), which relates the TD to the thermal capacity of the material. Indeed, the TD is the ratio between the heat conducted and the heat stored per unit volume. When the material is brought to a higher temperature, its heat capacity increases (value indicated table III). The decrease of TD with the measured temperature, with a given B_4C volume fraction, is almost identical for each B_4C content.

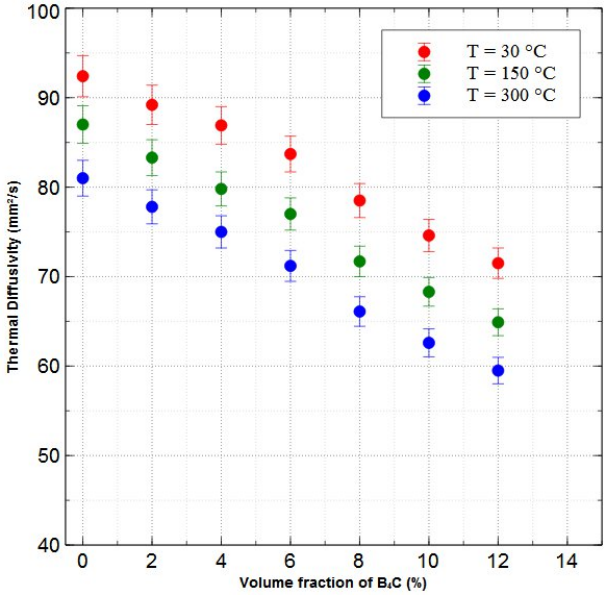

Figure 6. TD of Al/B_4C composites at different temperatures with different B_4C contents.

However, the TC of the composite materials is similar for the three temperatures due to the fact that Al has a slightly higher temperature conductivity, up to 300 °C [15] (Table III), and the TC of B_4C decreases, as shown in Table III. Fig. 7 shows the evolution of TC measured at 30 °C. The decrease of TC is due to the lower TC of B_4C with respect to Al. The decrease is rapid with a loss of 20% of TC when 12% B_4C is added in the Al

matrix.

The TC of composite materials can be estimated from theoretical models that are established under different conditions and take into account several variables [32], [33]. The theoretical TC of Al/B_4C was estimated using equation (3), as suggested by Hasselman-Johnson [34]. The model proposed by Hasselman and Johnson follows the general approach of Rayliegh and Maxwell, where the reinforcement is considered homogeneously diluted in the matrix. In this Hasselman-Johnson equation, the reinforcement is assumed to be spherical [32], [34]. It takes into account the intrinsic TC of the reinforcement and the matrix, the volume fraction of the reinforcement, the size of the reinforcement, and the interface thermal resistance.

$$k_c = \frac{2\left(\frac{k_r}{k_m}-\frac{k_r}{ah_c}-1\right)V_r+\left(2+\frac{k_r}{k_m}+\frac{2k_r}{ah_c}\right)}{\left(1-\frac{k_r}{k_m}+\frac{k_r}{ah_c}\right)V_r+\left(2+\frac{k_r}{k_m}+\frac{2k_r}{ah_c}\right)} \quad (4)\ [34]$$

where k is the TC, V is the volume fraction, a is the radius of reinforcement particles, and h_c is the interface thermal conductance.

This interface thermal barrier, also known the Kapitza resistance [35, 37], models the quality of the heat flow transfer according to the chemical nature of the two phases involved. Some studies have shown the importance of this interface thermal resistance on the modelling of TC of MMCs [35, 38]. Indeed, the thermal energy is conducted by different charge carriers such as electrons, ions, and holes for the electronic contribution and phonons for the contribution of the network. In the case of metals, electronic contribution is largely the majority, conversely, ceramics are essentially carried by the contribution of the network [39].

The heat flow through the Al-B_4C interface occurs by the electron-phonon interaction (e-p) within the matrix followed by the Al-phonon B_4C coupling (p-p) [35, 37]. The total interface thermal (R_{tot}) resistance can be defined by the sum of the internal thermal resistance of the coupling (R_{ep}) and by the resistance of the phonon-phonon coupling (R_{pp}) [35, 37]. Thermal resistance R_{ep} was estimated to be 8.9×10^{-10} K.m²/W for an Al/B_4C interface. The interface resistance R_{pp} is determined from the diffuse mismatch (DMM) model based on the density of the state of Debye phonons [37, 40]. The DMM model assumes that the phonons are all elastically scattered, and their transmission probability is proportional to the density of the state on the other side of the interface. R_{pp} is determined by the following relation:

$$R_{pp} = \frac{1}{h_{pp}} = \frac{4\times(C_r v_r + C_m v_m)}{C_m v_m C_r v_r} \quad (5)\ [35]$$

where C is the volumetric heat capacity and v is the Debye velocity. Index m and r correspond to matrix and reinforcement phase, respectively. From a microstructural point of view, we generally consider that an interface in direct contact between Al and B_4C is more representative than the interface comprising crystals of Al_2O_3 and Al_3BC. The Debye velocity (v_d) in the material is determined from the longitudinal (v_l) and transverse velocity (v_t) of Al and B_4C by the equation [36]:

$$v_d = \left\{\frac{1}{3}\left(\frac{1}{v_l^2}+\frac{2}{v_t^2}\right)\right\}^{-\frac{1}{2}} \quad (6)\ [36]$$

The calculated R_{pp} value is 6.2×10^{-10} K.m²/W. The total thermal resistance at the interface for an Al-B_4C interface from the DMM model is estimated ($R_{tot} = 1.5\times10^{-9}$ K.m²/W). The interface thermal conductance h_c representing the inverse of R_{tot} corresponds to 6.5×10^{8} W/m².K. All parameters are listed in Table IV.

Table IV: Physical parameters from literature for pure Al and pure B_4C

Materials	ρ (kg/m³)	v_l (m/s)	v_t (m/s)	v_d (m/s)	C (J/m³.K) at 30°C
Al	2710	6142 [36]	3100 [36]	3570	2.45×10^{6}
B_4C	2510	13951 [41]	8630 [41]	9685	2.44×10^{6}

The theoretical thermal conductivity calculated from the Hasselman-Johnson model, taking into account the interface thermal resistance estimated by the DMM model, is indicated by the black line (Fig. 7-a). In comparison, the displayed experimental values are lower than the theoretical ones. This behavior is associated with several phenomena. Firstly, the geometry of the reinforcement particles is considered as spherical, but the B_4C particles are random polygons with larger contact areas than those estimated in this model. Secondly, the heat transfer across the Al/B_4C interface is governed by the intrinsic properties of the Al/B_4C interface, which are given by its thermal conductance in this model. The dotted black line represents the thermal conductivity with a thermal conductance of 1×10^{5} W/m².K, which is the lowest thermal conductivity that can be consider for this system. According to Fig. 7-a, the model values are still much higher than the experimental thermal conductivity values, especially for B_4C with a volume fraction higher than 8%. Thirdly, the microstructure of the composite material should also be considered. Indeed, when the B_4C volume fraction increases, segregated B_4C particles are observed at the Al/Al grain boundaries, which can act as a barrier to the heat transfer inside the composite material. However, this point cannot be considered in the Hasselman-Johnson model. Finally, the last hypothesis is the formation of Al-B solid solution will decrease the thermal conductivity of the aluminum matrix. Viala [19] showed that boron can diffuse into the aluminum crystal lattice, with a solubility limit close to 0.02% - 0.045 at.% [16], [42]. The formation of these Al/B solid solutions should affect the Al matrix's thermal conductivity. The addition of elements in metals have shown adverse effects on the electrical and thermal conductivity properties [16]. Therefore, it can be hypothesized that the thermal conductivity of the Al matrix is reduced by the formation of Al/B solid solution; the Al TC further decreases with the increase in B concentration inside the Al matrix (equivalent to the volume fraction of B_4C) up to the limit of B solubility inside Al. Fig. 7-b shows the observed TC of the Al matrix (red-dotted curve) fitted with the theoretical values calculated using the modified Hasselman-Johnson model.

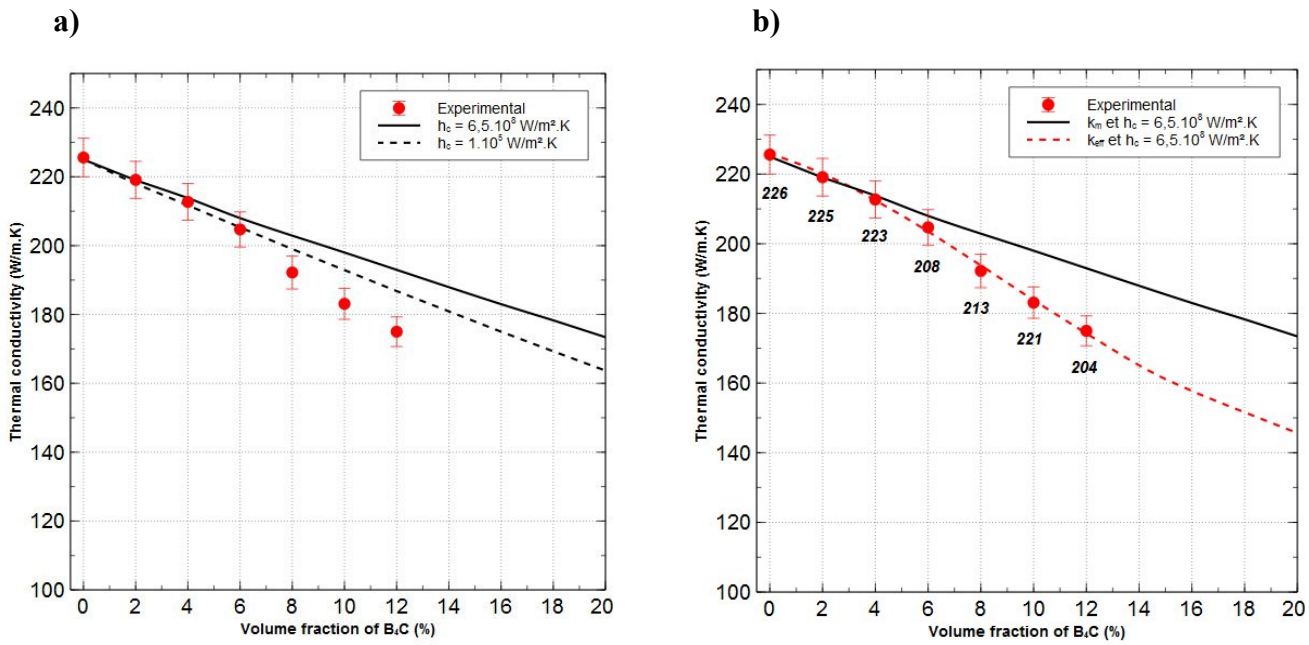

Figure 7. TC of Al/B_4C composites at 30 °C with different B_4C contents. Experimental points fitted with **(a)** the Hasselman-Johnson model and **(b)** the modified Hasselman-Johnson model.

3.2.2 Coefficient of thermal expansion (CTE) of Al/B_4C composite materials

The dimensional deformation of a body is generated during a temperature change and its amplitude depends on the crystallographic nature and inter-atomic interactions of the body. In the case of a two-phase composite material, matrix and reinforcement, the stiffness of one phase can limit the expansion of the other phase [7], [43]. The amplitude of the deformation depends on the shear transfer, which takes place at the matrix-reinforcement interface and demonstrates the importance of the nature of the cohesion between the two phases. These deformations can degrade the material by thermal or thermomechanical stress over time. Consequently, the induced deformation of the composite material depends strongly on the elastic constants of the different phases involved. Some models estimate the CTE of two-phase composite materials according to different simple factors, such as volume fraction, different elastic constants of the different phases [44]. Al, B_4C, and Al/B_4C composite materials have isotropic properties.

Fig. 8 shows the evolution of the CTE of Al/B_4C composite materials with different B_4C volume fractions. For each point, the experimental values are an average of the CTE in a temperature range of 50 °C to 250 °C.

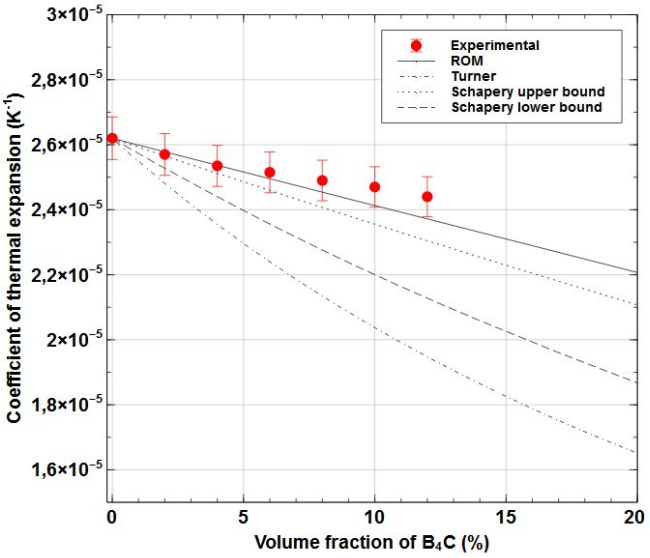

Figure 8. CTE of Al/B_4C composites between 50 °C and 250 °C with different B_4C contents.

To compare with the experimental CTE of the Al/B_4C, theoretical CTE are calculated using following models for a composite material:

Rule of mixture (ROM): $\alpha_c = \alpha_r V_r + \alpha_m V_m$ (7) [44]

Turner model: $\alpha_c = \frac{\alpha_m K_m V_m + \alpha_m K_m V_m}{K_m V_m + K_r V_r}$ (8) [44]

Schapery model: $\alpha_c = \alpha_r + (\alpha_m - \alpha_r)\frac{\left(\frac{1}{K_c}\right)-\left(\frac{1}{K_r}\right)}{\left(\frac{1}{K_m}\right)-\left(\frac{1}{Kr}\right)}$ (9) [45]

where, α is the CTE, V is the volume fraction, K is the bulk modulus, and c, m, and r indexes represent composite, matrix, and reinforcement phases, respectively.

The rule of mixture is the simplest to estimate thermal expansion of two-phase materials. Equation (7) was applied to composite materials that had close elastic constants [7, 44]. The upper bounds of different ROM models are also have been established in the literature. Turner's model is widely reported in the literature and used for MMCs. It is based on the fact that only uniform hydrostatic stresses exist in the phases. Hsieh *et al* [44] showed that Turner's model represented the lower limit of predicted CTE values. Schapery [45] employed potential energy principles of thermoelasticity theory to establish equation (9). A simple spherical shape is considered as homogeneously dispersed in the continuous phase. Through the Schapery model, the upper and lower bounds can be calculated using the upper and lower bounds of elastic modulus determined by Hashin and Shtrikman [46] and given in equation (10). The Schapery upper bound represents the Kerner model [47].

$$K_c^{(-)} = K_m + \frac{V_r}{\frac{1}{K_m - K_r} + \frac{V_m}{K_m + \frac{4}{3}G_m}} \quad (10)\ [47]$$

where G_m is the shear modulus of the matrix. By changing m and r indices in the equation, one can calculate the upper band of the Schapery composite modulus. While it's difficult to experimentally obtain K and G, these values can be estimated using the following equations [46]:

$$K = \frac{E}{3(1-2\nu)} \quad (11)\ [46]$$

$$G = \frac{E}{2(1+\nu)} \quad (12)\ [46]$$

where ν is Poisson's ratio. The mechanical characteristics of Al and B_4C are given in Table V.

Table V: Mechanical properties determined for pure Al and B_4C references

Materials	E (GPa)	K (GPa)	G (GPa)	*ν*
Al	69	67	26	0,33
B_4C	445	239	187	0,19

Fig. 8 shows that the average values of CTE ranged between 50 °C and 250 °C and slightly decrease when the volume fraction of B_4C increases. The CTE remained, higher than 24×10^{-6} K^{-1} up to 12 vol.% of B_4C. This trend is in accordance with the fact that the intrinsic CTE of B_4C ($5{,}5\times10^{-6}$ K^{-1}) is lower than Al ($26{,}2\times10^{-6}$ K^{-1}), leading to a continuous decrease of the Al/B_4C CTE with higher B_4C content.

The calculated theoretical CTEs of the Al/B_4C composites (α_c) in each model are indicated by the black lines in Fig. 8. In contrast with the TC, the theoretical model tends to be higher than the experimental values especially when the B_4C content increases. There is clearly a gap between the experimental values and the values calculated by the Turner model. The Schapery limits do not frame the experimental values of Al/B_4C composites. Rajendra *et al* [43] and Arpon *et al* [48] showed that the Schapery upper limit and the Turner model underestimate the CTE values of Al/B_4C and Al/SiC composites. However, we can see that the law of mixtures provides a better model of the thermo-mechanical behavior of our Al/B_4C composite materials. ROM is less often used because the nature of the cohesion between the matrix and reinforcement as well as stress transfer must be considered. Therefore, these phenomena require further investigation to understand the thermal expansion of our Al/B_4C composite materials.

Differences in CTE result from residual thermal stress during the fabrication of metal matrix composites with ceramic reinforcements. The amount of residual stresses depends on the volume fraction of the reinforcement and the type, shape, and size of the reinforcement used. These stresses form dislocations especially in the metal matrix, which is the most elastic phase. As these stresses affect the thermal and mechanical properties, the stress relaxation step is, therefore, important to annihilate these internal stresses. Indeed Shou-Yi Chang *et al* [49] observed that the CTE versus temperature curve evolved in three distinct parts in the case of ceramic reinforced composites. First, residual thermal stress restricted the thermal expansion of the composite; however, by increasing temperature, internal stress was almost eliminated and the CTEs of the composite reached higher values due to some matrix yielding and interfacial debonding. A. Fahmy [50] showed a similar behavior with discrepancies between theory and experiment linked to a lack of binding or coherency. When the composite was heated beyond the forming temperature, it expanded as though it were porous with essentially the same expansion coefficient as the matrix.

TEM analysis at the Al-B_4C interfacial zones show the quasi absence of chemical reactions even when no pores were observed at the Al-B_4C interfaces. Therefore, cohesion of Al-B_4C can only be considered by the shrinkage phenomenon, induced during cooling, due to the CTE difference between Al and B_4C. During the heating and cooling cycle, the materials showed no residual shrinkage, but this weak cohesion at the interface between Al and B_4C would induce a weak transfer of thermo-mechanical properties.

Due to the low cohesion and stress transfer between M-R, the thermal expansion of Al/B_4C composites mainly follows the contribution of Al by assimilating the B_4C reinforcement particles as porosities. Increasing the volume fraction of B_4C will lead to a continuous decrease in CTE. As a result, the experimental values of the CTE are higher than the models considering the elastic constants for the stress transfer at the M-R interface. The ROM model, free of the interface, more precisely predicts the evolution of the CTE of these Al/B_4C composites.

3.2 Mechanical properties

The enhancement of Al/B_4C properties were verified by comparing the macro-hardness and tensile tests of the Al/B_4C with the results from pure Al.

Fig. 9 presents the hardness over the volume content of B_4C. By adding B_4C reinforcement up to 12 vol.%, the hardness increased continuously. The hardness of a material represents its ease to deform under force. This deformation results from the mobility of dislocations, induced by the indentation, within its structure. For Al, the grain boundaries and the alumina layer represent breaks in the crystal lattice and slow down or block the mobility of dislocations. For the Al developed in this study, containing micrometer-sized Al grains, the hardness of the Al matrix was 24 HV. Increasing the B_4C content up to 12 vol.% caused up to a 200% linear increase in hardness, reaching a value of 50 HV.

This hardness improvement can be attributed to different factors [1]. The most important ones are: i) the B_4C reinforcement has a very high hardness, which creates a composite effect on the hardness of the composite; ii) a homogeneous distribution of the B_4C reinforcement in the Al matrix; iii) a good adhesion between the reinforcement and the matrix allowing for load transfer; and iv) generation of dislocations in the vicinity of the B_4C fillers in the deformed Al matrix. Concerning the linear evolution of hardness, this phenomenon has already been reported for Al/B_4C [24] and Al6061/B_4C [21] composites, only for B_4C content lower than 15 vol.%. In this, range (0-15 vol.%), the addition of small B_4C particles is sufficient to have a composite effect and increases the hardness but is not sufficient enough to generate a major change in the response behavior of the material.

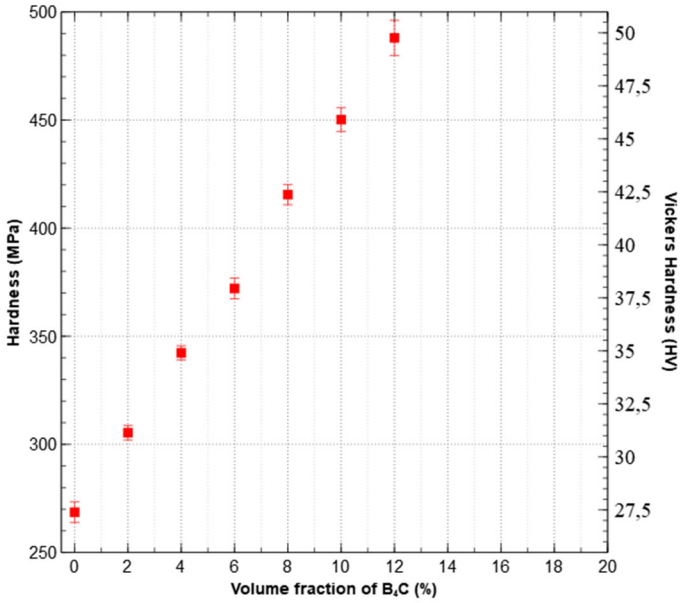

Figure 9. Macro-hardness of Al/B_4C composites with different B_4C contents.

Fig.10 displays the tensile true stress/true strain curves of Al/B_4C composites with varying B_4C contents. All tested composite materials show behavior which can be divided in two phases: a linear phase followed by a non-linear one. The transition between the two phases is continuous, without loss of stress and with the increase of strain. It can be called a transition phase with continuous tangent modulus. These curves indicate an elastic-plastic behavior with strain hardening. The first linear phase corresponds to the elastic behavior, and the second phase corresponds to the plastic behavior. The transition from the elastic to the plastic domain can be defined by the 0.2 % elastic limit σ_y, also called the strain hardening threshold. The hardening behavior can be described by the Ramberg-Osgood law.

Regarding all of the stress-strain curves, the addition of the B_4C reinforcement in volume has a direct impact on the overall mechanical behavior. First, the stiffness of the Al/B_4C composites slightly increase with higher proportions of B_4C in volume. This increase in stiffness is apparent in the elastic phase of the strain curves in Fig.10, between 0% and 2.5% of strain. Secondly, the value of the elastic limit σ_y increased with the addition of B_4C, changing from 58 ± 2 MPa to 78 ± 4 MPa and to 90 ± 1 MPa for pure Al, 6% of B_4C, and 12% of B_4C, respectively. This increase of the elastic limit corresponds to a gain of 55%. Thirdly, the addition of B_4C significantly reduced the plastic domain, reducing the plastic deformation from 31% to 6% for pure Al and 12% of B_4C, respectively. Moreover, during the hardening phase, pure Al and composites with lower proportions of B_4C ruptured and the stress decreased over a small range of the deformation. Hardening and softening occurred, while only hardening was present for higher percentage of B_4C. Fourthly, comparing the mechanical resistance and elongation at break, the addition of B_4C slightly increased the former and strongly decreased the latter, passing from 130 MPa to 140 MPa (+ 8%) for the UTS and from 31% to 9% (- 68%) for the elongation at break, for pure Al and 10 % of B_4C, respectively.

These changes of the behavior are also noticed in the fractured samples: for pure Al and lower addition of B_4C, the necking zone of the specimen appears while for highest proportions of B_4C, this zone of stricture becomes less and less important. The fracture changes from ductile to brittle whit the addition of B_4C. This brittleness of the material is due to the presence of B_4C. These results respect the rule of mixture, increasing the mechanical properties with the increasing of the reinforcement percentage. Moreover, these results are subjected to the good cohesion between the B_4C particles and the Al matrix.

Another important information is that UTS increases from 130 MPa for the raw Al to 150 MPa for the 8 vol.% of B_4C. For higher content, UTS decreases reaching a value of 120 MPa, lower than the Al matrix. This phenomenon has already been reported by Chen and Zhang [1], [24] for higher volume content and could be attributed to stress concentration at the Al-particles interfaces. For high volume content, particles rigidify the matrix and the latter cannot be deformed as it can for lower content. The load is then directly transferred to the interface. If the latter is weak, it breaks and provoke fracture.

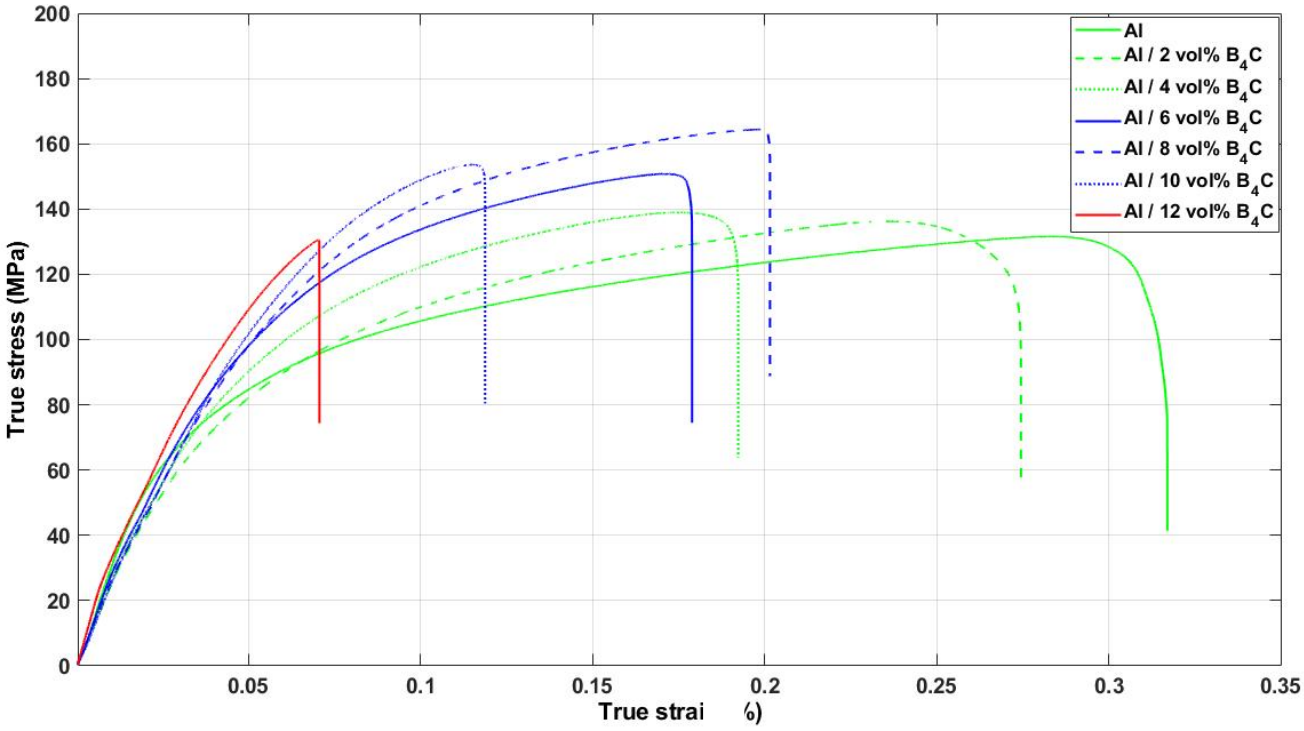

Figure 10. Tensile true stress true strain curves of Al/B_4C composite with different B_4C content

Table VI: Mechanical characteristics of Al/B_4C composite materials

	σ_y (MPa)	UTS (MPa)	A (%)	Z (%)
Al	58 ± 2	130 ± 2	31 ± 2	22 ± 4
Al/2%B_4C	65 ± 4	139 ± 2	26 ± 3	16 ± 4
Al/4%B_4C	75 ± 3	141 ± 6	19 ± 2	12 ± 1

Al/6%B_4C	78 ± 4	146 ± 5	16 ± 2	7 ± 1
Al/8%B_4C	80 ± 2	150 ± 10	10 ± 4	4 ± 1
Al/10%B_4C	85 ± 4	140 ± 5	9 ± 4	2 ± 0,5
Al/12%B_4C	90 ± 1	120 ± 5	6 ± 1	0,7 ± 0,2

4. Conclusion

Fully dense Al/B_4C composites were fabricated by solid state powder metallurgy, via hot-pressing, with B_4C volume fraction up to 12%. Fabrication process and conditions lead to an absence of 1) chemical reaction at the Al-B_4C interfacial zone and 2) the nucleation and growth of the AlB_2 phases inside the Al matrix. However, TEM analysis shows the presence of large Al_2O_3 precipitate which have to be linked with the presence of thin Al_2O_3 layer on the surface of the Al powders. The presence of these Al_2O_3 precipitate at the Al-Al grain boundaries and at the Al-B_4C interface is not yet understand.

TC of Al/B_4C composite materials is directly linked with the volume fraction of the B_4C particles. Indeed, TC significantly decrease as the B_4C content increase, with a loss of 20% at 12 vol.% B_4C. This decrease is correlated with the low TC of the B_4C particles. However, it has to be mentioned that, in the range of the B_4C content, TC of the Al/B_4C composite materials is higher than 170 W/m.K and remain stable whatever the temperature of measurement (30 °C 150 °C and 300 °C).

Hasselman-Johnson model was applied in order to calculate theoretical TC values of our Al/B_4C composite materials. For B_4C volume fraction higher than 4% theoretical TC values are higher than measured TC whatever the interfacial thermal resistance value used in this model. Therefore, interfacial thermal resistance cannot be used as adapt parameters to fit theoretical and experimental values. We propose that the diffusion of B inside the Al matrix, during the elaboration process, lead to formation of Al-B solid solution which obviously have TC lower than pure Al. If we assume that the diffusion of B is linked with the volume fraction of B_4C we can module the TC of Al-B matrix and fit experimental and theoretical TCs.

TEM analysis at the Al-B_4C interfacial zones show the quasi absence of 1) chemical reactions and 2) pores at the Al-B4C interfaces. Therefore, Al-B_4C interfacial adhesion can only be induced by shrinkage phenomenon (difference of CTE between Al and B_4C), induced during cooling. This weak interfacial cohesion between Al and B4C leads to weak transfer of thermo-mechanical properties and CTE values mower than theoretical one calculated by theoretical models.

As demonstrated previously, incorporation of B_4C content in Al matrix improves mechanical performance. In our materials we also observed an increase, up to 8 vol.% B_4C, of mechanical properties which a decrease of the elongation at rupture. The strain hardening threshold and the UTS strength increased up to 37% and 13%, respectively. A second behavior appeared for 10 vol.% and 12 vol.% where the material become more and more brittle, leading to very limited plastic phases with a continuous decrease in the elongation at break but

under lower stresses, even lower than pure aluminum for 12% B_4C. This behavior is related to the accumulation of B_4C particles, whose cohesion between them is absent, propagating the cracks until an advanced rupture.

The quality of the interface shows its importance in the transfer of physical and mechanical properties of Al/B_4C composites. The materials elaborated by powder metallurgy under the conditions of this study showed insufficient cohesion to promote significant improvements of the thermal-mechanical properties. Moreover, the incorporation of B_4C reinforcements leads to an opposite evolution of the thermal and mechanical properties.

Acknowledgments

The authors are pleased to acknowledge support from ORANO company, the Centre National de la Recherche Scientifique (CNRS), the laboratories: Institut de Chimie de la Matière Condensée de Bordeaux (ICMCB), Laboratoire Génie de Production (LGP), Institut Pprime; and the University of Bordeaux for this research. This work partially pertains to the French Government program "Investissements d'Avenir" (LABEX INTERACTIFS, reference ANR-11-LABX-0017-01). This work has been partially supported by « Nouvelle Aquitaine » Region and by European Structural and Investment Funds (ERDF reference: P-2016-BAFE-94/95).

References

[1] H. S. Chen, W. X. Wang, Y. L. Li, J. Zhou, H. H. Nie, and Q. C. Wu, The design, microstructure and mechanical properties of B_4C/6061Al neutron absorber composites fabricated by SPS, *Materials & Design*, **vol. 94**, (2016), p. 360-367, doi: 10.1016/j.matdes.2016.01.030.

[2] X.-G. Chen, M. da Silva, P. Gougeon, and L. St-Georges, Microstructure and mechanical properties of friction stir welded AA6063–B_4C metal matrix composites, *Materials Science and Engineering: A*, **vol. 518**, (2009), 1-2, p. 174-184, doi: 10.1016/j.msea.2009.04.052.

[3] Y. Z. Li, Q. Z. Wang, W. G. Wang, B. L. Xiao, and Z. Y. Ma, Effect of interfacial reaction on age-hardening ability of B_4C/6061Al composites, *Materials Science and Engineering: A*, **vol. 620**, (2015) p. 445-453, doi: 10.1016/j.msea.2014.10.025.

[4] D. Miracle, Metal matrix composites – From science to technological significance, *Composites Science and Technology*, **vol. 65**, (2005), 15-16, p. 2526-2540, doi: 10.1016/j.compscitech.2005.05.027.

[5] P. Zhang, Y. Li, W. Wang, Z. Gao, and B. Wang, The design, fabrication and properties of B_4C/Al neutron absorbers, *Journal of Nuclear Materials*, **vol. 437**, (2013),1-3, p. 350-358, doi: 10.1016/j.jnucmat.2013.02.050.

[6] J.-F. Silvain, J.-M. Heintz, and A. Veillere, Matériaux composites à matrices métalliques, *Techniques de l'Ingénieur*, (2018), p. 21.

[7] G. Khare, N. Chandra, and J.-F. Silvain, Application of Eshelby's Tensor and Rotation Matrix for the Evaluation of Thermal Transport Properties of Composites, *Mechanics of Advanced Materials and Structures*, **vol. 15**, (2008), 2, p. 117-129, doi: 10.1080/15376490701810464.

[8] S. P. Dwivedi, A. Saxena, S. Sharma, G. Singh, J. Singh, M. Mia, S. Chattopadyaya, A. Pramanik, D. Y. Pimenov, S. Wojciechowski., Effect of ball-milling process parameters on mechanical properties of Al/Al2O3/collagen powder composite using statistical approach, *Journal of Materials Research and*

Technology, vol. 15, (2021), p. 2918-2932, doi: 10.1016/j.jmrt.2021.09.082.
[9] S. Sharma, J. Singh, M. K. Gupta, M. Mia, S. P. Dwivedi, A. Saxena, S. Chattopadhyaya, R. Singh, D. Y. Pimenov, M. E. Korkmaz., Investigation on mechanical, tribological and microstructural properties of Al–Mg–Si–T6/SiC/muscovite-hybrid metal-matrix composites for high strength applications, *Journal of Materials Research and Technology*, vol. 12, (2021), p. 1564-1581, doi: 10.1016/j.jmrt.2021.03.095.
[10] K. Ma, E. J. Lavernia, and J. M. Schoenung, Particulate reinforced aluminum alloy matrix composites - a review on the effect of microconstituents, *Reviews on Advanced Materials Science*, p. 14, (2017).
[11] F. A. Girot, J. M. Quenisset, and R. Naslain, Discontinuously-reinforced aluminum matrix composites, *Composites Science and Technology*, **vol. 30**, (1987), 3, p. 155-184, doi: 10.1016/0266-3538(87)90007-8.
[12] S. Hayun, S. Kalabukhov, V. Ezersky, M. P. Dariel, and N. Frage, Microstructural characterization of spark plasma sintered boron carbide ceramics, *Ceramics International*, p. 7, (2010).
[13] F. Thévenot, Boron Carbide A Comprehensive Review, *Journal of the European Ceramic Society*, p. 21, (1990).
[14] R. Develay, Aluminium non allié, *Techniques de l'ingénieur*, p. 25, (1989).
[15] C. Vargel, Propriétés générales de l'aluminium and de ses alliages, *Techniques de l'ingénieur*, p. 19, (2005).
[16] C. Vargel, Métallurgie de l'aluminium, *Techniques de l'ingénieur*, p. 27, (2010).
[17] J. Jung et S. Kang, Advances in Manufacturing Boron Carbide-Aluminum Composites, *Journal of the American Ceramic Society*, vol. 87, (2004), 1, p. 47-54, doi: 10.1111/j.1551-2916.2004.00047.x.
[18] J. M. Torralba, C. E. da Costa, and F. Velasco, P/M aluminum matrix composites: an overview, *Journal of Materials Processing Technology*, **vol. 133**, (2003), 1-2, p. 203-206, doi: 10.1016/S0924-0136(02)00234-0
[19] . C. Viala, J. Bouix, G. Gonzalez, and C. Esnouf, Chemical reactivity of aluminium with boron carbide, Journal of Material Science, **vol. 32**, (1997), p. 15.
[20] Z. Zhang, K. Fortin, A. Charette, and X.-G. Chen, Effect of titanium on microstructure and fluidity of Al–B_4C composites, *J Mater Sci*, **vol. 46**, (2011), 9, p. 3176-3185, doi: 10.1007/s10853-010-5201-1.
[21] H. Guo, Z. Zhang, Y. Zhang, Y. Cui, L. Sun, et D. Chen, Improving the mechanical properties of B_4C/Al composites by solid-state interfacial reaction, *Journal of Alloys and Compounds*, vol. 829, (2020), p. 154521, doi: 10.1016/j.jallcom.2020.154521.
[22] C.-L. Yeh et C.-Y. Ke, Intermetallic/Ceramic Composites Synthesized from Al–Ni–Ti Combustion with B4C Addition, *Metals*, vol. 10, (2020), 7, p. 873, doi: 10.3390/met10070873.
[23] D. Lee, J. Kim, B. Park, I. Jo, S. Lee, Y. Kim, S. Lee, S. Cho, Mechanical and Thermal Neutron Absorbing Properties of B_4C/Aluminum Alloy Composites Fabricated by Stir Casting and Hot Rolling Process, *Metals*, vol. 11, (2021), 3, p. 413, doi: 10.3390/met11030413.
[24] L. Zhang, Z. Wang, Q. Li, J. Wu, G. Shi, F. Qi, X. Zhou, Microtopography and mechanical properties of vacuum hot pressing Al/B_4C composites, *Ceramics International*, **vol. 44**, (2018), 3, p. 3048-3055, doi: 10.1016/j.ceramint.2017.11.065
[25] M. S. Soliman, M. M. El Rayes, A. T. Abbas, D. Yu. Pimenov, I. N. Erdakov, et H. Junaedi, Effect of tensile strain rate on high-temperature deformation and fracture of rolled Al-15 vol% B_4C composite, *Materials Science and Engineering: A*, vol. 749,(2019), p. 129-136, doi: 10.1016/j.msea.2019.02.016.
[26] B. Basu, G. B. Raju, et A. K. Suri, Processing and properties of monolithic TiB_2 based materials, *International Materials Reviews*, vol. 51, (2006), 6, p. 352-374, doi: 10.1179/174328006X102529.
[27] M. Munro, Evaluated Material Properties for a Sintered alpha-Alumina, *Journal of the American Ceramic Society*, vol. 80, (2005), 8, p. 1919-1928, doi: 10.1111/j.1151-2916.1997.tb03074.x.
[28] R. G. Munro, Material Properties of a Sintered α-SiC, *Journal of Physical and Chemical Reference Data*, vol. 26, (1997), 5, p. 1195-1203, doi: 10.1063/1.556000.
[29] T. Ohji, Y. Yamauchi, W. Kanematsu, et S. Ito, Tensile Rupture Strength and Fracture Defects of Sintered Silicon Carbide, *J American Ceramic Society*, vol. 72, (1989) 4, p. 688-690, doi: 10.1111/j.1151-2916.1989.tb06198.x.
[30] Y. T. Zhou, Y.N Zan, S.J. Zheng, Q.Z. Wang, B.L. Xiao, Distribution of the microalloying element Cu in B_4C-reinforced 6061Al composites, *Journal of Alloys and Compounds*, **vol. 728**, (2017), p. 112-117,

doi: 10.1016/j.jallcom.2017.08.273.
[31] Mathias Georges, Approche du frittage SPS de céramiques fines de carbure de bore: rôle des poudres initiales and de la mise en forme, *Thesis*, (2016), Université de Limoges, Limoges, France
[32] K. Pietrak and T. S. Wisniewski, A review of models for effective thermal conductivity of composite materials, *Journal of Power Technologies*, (2015), p. 11.
[33] R. C. Progelhof, J. L. Throne, and R. R. Ruetsch, Methods for predicting the thermal conductivity of composite systems: A review, *Polym. Eng. Sci.*, **vol. 16**, (1976), 9, p. 615-625, doi: 10.1002/pen.760160905.
[34] D. P. H. Hasselman and L. F. Johnson, Effective Thermal Conductivity of Composites with Interfacial Thermal Barrier Resistance, *Journal of Composite Materials*, **vol. 21**, (1987) 6, p. 508-515, doi: 10.1177/002199838702100602.
[35] M. Battabyal, O. Beffort, S. Kleiner, S. Vaucher, and L. Rohr, Heat transport across the metal–diamond interface, *Diamond and Related Materials*, **vol. 17**, (2008) 7-10, p. 1438-1442, doi: 10.1016/j.diamond.2008.01.023.
[36] M. Kida, L. Weber, C. Monachon, and A. Mortensen, Thermal conductivity and interfacial conductance of AlN particle reinforced metal matrix composites, *Journal of Applied Physics*, **vol. 109**, (2011), 6, p. 064907, doi: 10.1063/1.3553870.
[37] A. Majumdar and P. Reddy, Role of electron–phonon coupling in thermal conductance of metal–nonmetal interfaces, *Appl. Phys. Lett.*, **vol. 84**, (2004), 23, p. 4768-4770, doi: 10.1063/1.1758301.
[38] S. Polat, Y. Sun, E. Çevik, and H. Colijn, Evaluation of thermal conductivity of GNPs-doped B_4C/Al-Si composites in terms of interface interaction and electron mobility, *Diamond and Related Materials*, **vol. 98**, (2019), p. 107457, doi: 10.1016/j.diamond.2019.107457.
[39] J.-P. Issi, Mécanismes de conduction thermique dans les solides : des métaux aux isolants, *Rev. Met. Paris*, **vol. 96**, (1999), 5, p. 575-584, doi: 10.1051/metal/199996050575.
[40] L. De Bellis, P. E. Phelan, and R. S. Prasher, Variations of Acoustic and Diffuse Mismatch Models in Predicting Thermal-Boundary Resistance, *Journal of Thermophysics and Heat Transfer*, **vol. 14**, (2000), 2, p. 144-150, doi: 10.2514/2.6525.
[41] P. A. Medwick, H. E. Fischer, and R. O. Pohl, Thermal conductivity and specific heat of boron carbides, *Journal of Alloys and Compounds*, **vol. 203**, (1994), p. 67-75, doi: 10.1016/0925-8388(94)90716-1.
[42] H. Duschanek and P. Rogl, The Al-B (Aluminum-boron) System, *Journal of Phase Equilibria*, **vol. 15**, (1994), 5.
[43] R. U. Vaidya and K. K. Chawla, Thermal expansion of metal-matrix composites, *Composites Science and Technology*, **vol. 50**, (1994), 1, p. 13-22, doi: 10.1016/0266-3538(94)90122-8.
[44] C. L. Hsieh and W. H. Tuan, Thermal expansion behavior of a model ceramic–metal composite, *Materials Science and Engineering: A*, **vol. 460-461**, (2007), p. 453-458, doi: 10.1016/j.msea.2007.01.109.
[45] R. A. Schapery, Thermal Expansion Coefficients of Composite Materials Based on Energy Principles, *Journal of Composite Materials*, **vol. 2**, (1968), 3, p. 380-404, doi: 10.1177/002199836800200308.
[46] Y. Zare and K. Y. Rhee, Development of Hashin-Shtrikman model to determine the roles and properties of interphases in clay/CaCO3/PP ternary nanocomposite, *Applied Clay Science*, **vol. 137**, (2017), p. 176-182, doi: 10.1016/j.clay.2016.12.033.
[47] M. Tayebi, M. Jozdani, and M. Mirhadi, Thermal expansion behavior of Al–B_4C composites by powder metallurgy, *Journal of Alloys and Compounds*, **vol. 809**, (2019), p. 151753, doi: 10.1016/j.jallcom.2019.151753.
[48] R. Arpón, J. M. Molina, R. A. Saravanan, C. García-Cordovilla, E. Louis, and J. Narciso, Thermal expansion behaviour of aluminium/SiC composites with bimodal particle distributions, *Acta Materialia*, **vol. 51**, (2003), 11, p. 3145-3156, doi: 10.1016/S1359-6454(03)00126-5.
[49] .-Y. Chang, S.-J. Lin, and M. C. Flemings, Thermal expansion behavior of silver matrix composites, *Metall and Mat Trans A*, **vol. 31**, (2000), 1, p. 291-298, doi: 10.1007/s11661-000-0073-7.
[50] A. A. Fahmy and A. N. Ragai, Thermal ‐ Expansion Behavior of Two ‐ Phase Solids, *Journal of Applied Physics*, **vol. 41**, (1970), 13, p. 5108-5111, doi: 10.1063/1.1658619.

Nomenclature

A = Elongation (%)

a = Radius of reinforcement particle (m)

Al = Aluminum

AlB_2 = Diboride Aluminum

Al_2O_3 = Alumina

Al_3BC = Alumino boron carbide

AMC = Aluminum Matrix Composite

B_4C = Boron carbide

C_i = Volumetric heat capacity ($J/m^3.K$)

C_p = Heat capacity (J/kg.K)

CTE = Coefficient of Thermal Expansion

D = Average dimensions of the diagonals imprit (m)

DMM = Diffuse Mismtach Model

E = Young modulus (GPa)

EDX = Energy Dispersive X-ray spectroscopy

F = Force (N)

FIB = Focused Ion Beam

G = Shear modulus (MPa)

HAADF = High-Angle Annular Dark-Field imaging

h_c = Interface thermal conductance ($W/m^2.K$)

HV = Hardness Vickers

K_i = Bulk modulus (MPa)

k_i = Thermal conductivity (W/m.K)

M = Matrix

MMC = Metal Matrix Composite

R = Reinforcement

R_{ep} = Resistance of electrons-phonons coupling ($K.m^2/W$)

ROM = Rules of mixture

R_{pp} = Resistance of phonons-phonons coupling ($K.m^2/W$)

R_{tot} = Resistance total ($K.m^2/W$)

SEM = Scanning Electronic Microscopy

SiC = Silicon carbide

T = Temperature (K)

TC = Thermal Conductivity

TD = Thermal Diffusivity

TEM = Transmission Electronic Microscopy

TiB_2 = Diboride titanium

TiO_2 = Dioxide titanium

UTS = Ultimate Tensile Strength (MPa)

V_i = Volumic fraction

υ_i = Phonon velocity in materials (m/s)

Z = Striction (%)

α = Coefficient of thermal expansion (K^{-1})

λ = Thermal conductivity (W/m.K)

ρ = Density (g/cm^3)

σ_y = Strain hardening threshold (MPa)

ν = Poisson coefficient

Subscript

c = composite

l = longitudinal

m = matrix

r = reinforcement

t = transversal

Table caption

Table I : Mechanical characteristics of ceramic reinforcement

Table II : Material chemistry of Aluminum and Boron carbide powders

Table III : Physical properties determined for pure Al and pure B_4C

Table IV: Physical parameters from literature for pure Al and pure B_4C

Table V: Mechanical properties determined for pure Al and B_4C references

Table VI : Mechanical characteristics of Al/B_4C composite materials

Figure caption